arXiv:1208.5963v1 [math.DS] 29 Aug 2012

How far are vowel formants from computed vocal tract resonances?

D. Aalto[1,3], A. Huhtala[2], A. Kivelä[2], J. Malinen[2],
P. Palo[3], J. Saunavaara[4], M. Vainio[3]

[1] Dept. of Signal Processing and Acoustics, Aalto University, Finland

[2] Dept. of Mathematics and Systems Analysis, Aalto University, Finland

[3] Inst. of Behavioural Sciences (SigMe group), University of Helsinki, Finland

[4] Medical Imaging Centre of Southwest Finland

jarmo.malinen@aalto.fi

December 2, 2019

Abstract

We compare numerically computed resonances of the human vocal tract with formants that have been extracted from speech during vowel pronunciation. The geometry of the vocal tract has been obtained by MRI from a male subject, and the corresponding speech has been recorded simultaneously. The resonances are computed by solving the Helmholtz partial differential equation with the Finite Element Method (FEM).

Despite a rudimentary exterior space acoustics model, i.e., the Dirichlet boundary condition at the mouth opening, the computed resonance structure differs from the measured formant structure by ≈ 0.7 semitones for [i] and [u] having small mouth opening area, and by ≈ 3 semitones for vowels [a] and [æː] that have a larger mouth opening. The contribution of the possibly open velar port has not been taken into considaration at all which adds the discrepancy for [a] in the present data set. We conclude that by improving the exterior space model and properly treating the velar port opening, it is possible to computationally attain four lowest vowel formants with an error less than a semitone. The corresponding wave equation model on MRI-produced vocal tract geometries is expected to have a comparabale accuracy.

Keywords. Formant analysis, acoustic resonance computation, FEM, MRI.

1 Introduction

The purpose of this paper is to evaluate the accuracy of vowel simulations based on the wave equation model (1). We use 3D vocal tract (VT) geometries that have been obtained by Magnetic Resonance Imaging (MRI) from a native male speaker of Finnish while he pronounces prolonged vowels [ɑ], [i], [u], and [œ]. The evaluation is carried out by comparing the computed resonances of (1) with the measured formants, extracted from sound samples, instead of comparing simulated and actual speech signals. In this work, *the sound samples have been recorded simultaneously with the MRI*, using the equipment and the arrangements detailed in [5, 6, 21, 27]. This is in contrast to, e.g., our earlier work [15] where only a single anatomic configuration (corresponding to Swedish [ø]) was taken from the data set of [13].

We use the same wave equation model for vowels as in [15], namely

$$\begin{cases} \Phi_{tt} = c^2\Delta\Phi \text{ on } \Omega, \Phi = 0 \text{ on } \Gamma_1, \\ \frac{\partial\Phi}{\partial\nu} = 0 \text{ on } \Gamma_2, \Phi_t + c\frac{\partial\Phi}{\partial\nu} = 2\sqrt{\frac{c}{\rho_0}}u \text{ on } \Gamma_3, \end{cases} \tag{1}$$

where $\Omega \subset \mathbb{R}^3$ is the interior of the VT whose boundary $\partial\Omega = \overline{\Gamma_1} \cup \overline{\Gamma_2} \cup \overline{\Gamma_3}$ consists of the mouth opening Γ_1, the VT tissue walls Γ_2, and an (imaginary) control surface Γ_3 placed right above the glottis. The parameters $c = 350$ m/s and $\rho_0 = 1.225$ kg/m^3 are the speed of sound in and the density of dry air at $T = 305$ K, respectively. The functions in (1) are as follows: $u = u(\mathbf{r}, t)$ is the incoming acoustic power (per unit area) at glottis input, $\frac{\partial\Phi}{\partial\nu} = \nu \cdot \nabla\Phi$, and ν is the exterior unit normal on $\partial\Omega$. In time domain simulations, we compute the velocity potential $\Phi(\mathbf{r}, t)$ for a given glottal input function $u(\mathbf{r}, t)$ produced by a source such as described in [2, 3]. From the velocity potential, the sound pressure and (perturbation) velocity can be extracted as the partial derivatives $p' = \rho_0\Phi_t$ and $\mathbf{v} = \nabla\Phi$. The physics of model (1) is further explained in [15] and the references therein.

In the past, the VT acoustics has been modelled in many different ways. Electrical *transmission lines* have been used already in [10], and the classical *Kelly–Lochbaum model* in [17] makes use of reflection/transmission coefficients of a variable diameter tube. The 3D *wave equation* for linear wave propagation as well as the related *Helmholtz equation* for acoustic resonances have been known for a long time; see, e.g. [16]. The Kelly–Lochbaum model is closely related to *Webster's equation* in, e.g., [7, 14] but the latter can be easily deduced from variable-impedance electrical transmission lines as well as from the wave equation in 3D tubular domains as shown in great generality in [19]. More advanced models are the *transmission line networks* that

have been applied for speech in, e.g., [11, 12, 22]; see also [4] for a purely mathematical treatment.

At their best, all of these modelling paradigms are known to produce very good simulated speech even though they are based on radically simplified representations of the underlying anatomic geometry Ω with the sole exception of the wave equation. In most applications, simplifications are even desirable as it may improve conceptual clarity and reduce computational burden. There are, however, situations where the faithful representation of the VT geometry is required, e.g., when modelling the effects of anatomical abnormalities and maxillofacial surgery on speech [8, 23, 25, 32, 33, 34].

2 Background and motivation

In our earlier work [15], the same numerical computations were carried out using a minimal data set: a single MRI-based anatomic geometry Ω corresponding to the Swedish vowel [ø]. The computed resonances were compared to the first four formants of all Swedish vowels (including [ø]) that were extracted from speech samples of the same test subject. The speech samples were not recorded simultaneously with the MRI because of technological restrictions but the subject was in a similar supine position during both MRI and speech recording; see [13].

We made the following observations in [15]:

1. The computed resonances $R_1 ... R_4$ corresponding the formants $F_1 ... F_4$ of [ø] are systematically $3\frac{1}{2}$ semitones too high compared to the measured values;

2. the *formant ratios* of the computed and measured data (i.e., R_i/R_1 and F_i/F_1 for $i = 2, 3, 4$) correspond to each other quite well; and

3. if the systematic error in $R_1 ... R_4$ of [ø] is compensated by linear scaling, then the scaled, computed data gets identified correctly as [ø] in the measured formant table from the same subject.

Two main potential sources were identified for the discrepancy: (i) the Dirichlet boundary condition on Γ_1 in (1) results in *too short acoustic length of the computational VT*; and (ii) the minimal *data set used in [15] is insufficient* to draw any conclusions on the error sources. The purpose of this work is to exclude the latter possibility (ii) by extending and improving the data set in an essential manner. We also aim at a deeper understanding of the sources of descrepancy to guide future model improvements and to understand the quality of simulation that one can reasonably expect to attain.

We remark that the formant computation of [15] was later validated by completely independent FEM resonance computations that were based on the generalized Webster's model instead of (1); the computed resonances corresponding to $F_1 ... F_4$ were practically the same as reported in [1, Table 3.1 on p. 31]. As shown in [19], the generalized Webster's model is a low-frequency approximation of the wave equation in a tubular domain. In the case of human VT, the approximation remains accurate for formants $F_1 ... F_3$ and even for F_4 at least in some vowel configurations where cross-mode resonances do not dominate; see [15, Fig. 1].

We comment on the interesting parallel work [32] at the end of the paper.

3 Model and methods

As explained in [15, p. 3], the resonances of Eq. (1) can be solved by finding the complex frequencies λ such that the Helmholtz problem

$$\begin{cases} \lambda^2 \Phi_\lambda = c^2 \Delta \Phi_\lambda \text{ on } \Omega, \Phi_\lambda = 0 \text{ on } \Gamma_1, \\ \frac{\partial \Phi_\lambda}{\partial \nu} = 0 \text{ on } \Gamma_2, \text{ and } \lambda \Phi_\lambda + c \frac{\partial \Phi_\lambda}{\partial \nu} = 0 \text{ on } \Gamma_3 \end{cases} \tag{2}$$

is solvable for some nonzero eigenfunctions $\Phi_\lambda(\mathbf{r})$. It is known that all such eigenvalues λ form an infinite sequence $\{\lambda_j\}_{j \in \mathbb{Z} \setminus \{0\}}$ with $|\lambda_j| \to \infty$ as $|j| \to \infty$, $Re\, \lambda_j \leq 0$, and $Im\, \lambda_{-j} = -Im\, \lambda_j$. The lowest formants F_1, F_2, ..., correspond to the numbers $R_j = Im\, \lambda_j$ for $j = 1, 2, \ldots$ in the order of increasing imaginary parts.

As solving Eqs. (1) and (2) analytically is possible only in a radically simplified geometry [31], we solved the problem numerically by the *Finite Element Method* (FEM). This is the approach used in [18], [24], [9], [29], [35], and by many others. Eqs. (2) were solved in variational form as given in [15, Eq. (5)] using a custom implementation of FEM programmed in MATLAB. We used piecewise linear shape functions on tetrahedral meshes. The tetrahedral meshes were generated using TetGen [30] from a triangular surface mesh. As a result, we obtained the matrices $\boldsymbol{A}$ and $\boldsymbol{B}$ for a high-order eigenvalue problem $\boldsymbol{A}\boldsymbol{y}(\lambda) = \lambda \boldsymbol{B}\boldsymbol{y}(\lambda)$ as explained in [15, Eq. (6)]. The lowest eigenvalues λ_j, $j = 1, 2, 3, 4$ were then computed using the *eigs* routine of MATLAB. It takes around 3 seconds on a workstation with an Intel Xeon X3450 processor to build the matrices and to solve the eigenvalue problem.

The imaginary parts of the computed λ_j are given in Table 1 together with the number of elements used in each VT geometry. The computed values are good approximations of the eigenvalues defined in Eqs. (2) when the number of elements is high enough. It was observed with the anatomic

geometry of [u] that using four times as many elements does not change the numerical result, and thus the resonances given in Table 1 can be regarded as accurate in this respect.

Vowel	R_1	R_2	R_3	R_4	# of elem.
[ɑ]	720	1547	2721	4138	47514
[i]	246	2135	3592	4667	37335
[u]	324	659	2262	3091	50579
[œ]	562	1612	2519	3602	53087

Table 1: *Resonances (in Hz) of the Helmholtz problem* (2) *by FEM, and the number of the elements in each geometry.*

4 Geometric data from MRI

The raw MRI data was collected from a native male Finnish speaker while he pronounced prolonged vowels [ɑ], [i], [u], and [œ] in a supine position.

As a result of these pilot experiments in June 2010, a combined data set of 53 simultaneously recorded MRI data and sound samples was produced. Out of this data set, four samples were chosen based on a visual quality assessment of spectrogram data as well as the requirement that the F_1-F_2 vowel space should be covered in a satisfactory manner. The spectrograms of these samples can be found in [27, p.64, p.66, p.68, and p.79]. The first three of these samples were pronounced at the fundamental frequency $f_0 = 110$ Hz and the last one at $f_0 = 137.5$ Hz.

A Siemens Magnetom Avanto 1.5T scanner was used in these experiments. A 12-element Head Matrix Coil was combined with a 4-element Neck Matrix Coil in order to cover the anatomy of interest. 3D VIBE (Volumetric Interpolated Breath-hold Examination) [28] was found out to be the most suitable MRI sequence for rapid 3D acquisition. As the naming of the sequence suggests, it was originally developed for fast 3D imaging of the abdominal region where breath-hold during the scan is essential. Sequence parameters were optimized in order to minimize the acquisition time, and we were able to carry out MRI with 1.8 mm isotropic voxels in just 7.6 s.

The tissue/air interface from the MR data was extracted by combining sagittal DICOM sequence -images to form a 3D voxel image. A triangular surface mesh of the interface was then extracted using custom MATLAB code. The three boundary components Γ_1, Γ_2, and Γ_3 were identified manually in the triangle mesh so that the different boundary conditions could

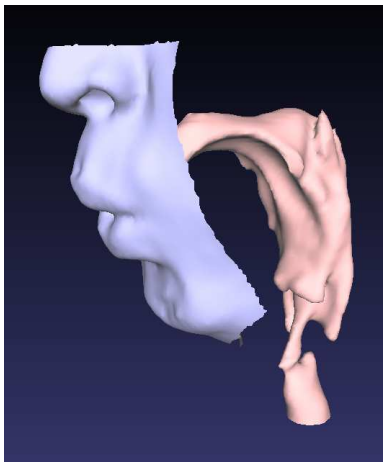


Figure 1: *Air/tissue interface of the test subject while pronouncing [y]. The nasal cavities have been excluded.*

be applied in right places. Since teeth are not visible in MRI (and hence, they are not part of the computational geometry of this work), some resulting artefacts had to be corrected manually. The velar port was open in the geometries of [ɑ] and [i], and the resulting hole in the surface model was manually closed. A shaded representation of a typical surface mesh is presented in Fig. 1.

The geometric error in the tissue/air interface is a fraction of the voxel-based resolution of the original MRI data: interpolating in 2D sections by the gray-scale values of pixels results in about 1.8 bits of additional information compared to the MRI pixel size, corresponding to the geometric error of $\approx$ 0.5 mm with the current voxel size of 1.8 mm; see [6]. We conclude that the resonances in Table 1 do not contain essential errors due to inaccuracies of surface geometries.

5 Sound recording and formant extraction

The interior of a MRI machine is a challenging environment for speech recording. We used the recording arrangement discussed in [21, 27] and the experimental arrangements described in [5, Section 2]; see also [6].

Let us briefly describe the recording arrangement. A two-channel sound collector samples the speech and noise signals in a dipole configuration. The sound collector is an acoustically passive, non-microphonic device which does not cause artifacts in the MR images. The sound signals are coupled to a RF-shielded microphone array by acoustic waveguides of length 3 m. There

are acoustic impedance terminations at the both ends of the waveguides to sufficiently reduce longitudinal resonances. The microphone signals are coupled to an amplifier that is situated outside the MRI room. This analogue electronics is used to optimally subtract the noise signal from the contaminated speech signal in real time, and the cleaned-up signal is fed back to test subject's earphones. The same audio signal is digitized by a 24bit ADC, and the residual longitudinal resonances of the waveguides are compensated numerically in the post-processing stage.

Vowel	F_1	F_2	F_3	F_4
[ɑ]	651 ± 7	1024 ± 35	2647 ± 117	3679 ∓ 36
[i]	247 ± 9	2183	3304 ∓ 46	4407 ∓ 251
[u]	306 ∓ 37	675 ∓ 39	2173 ± 13	3242 ± 139
[œ]	483 ∓ 35	1249 ± 74	1994 ∓ 50	3188 ∓ 17

Table 2: *Formants (in Hz) computed as means of those extracted from the beginnings and ends of the samples. The upper (lower) sign refers to the beginning (resp., the end) of the sample.*

For this work, the formants $F_1 ... F_4$ were first extracted separately from the beginnings and the ends of the sound samples where the acoustic MRI noise is absent. The extraction was done by LPC using MATLAB similarly to the approach explained in [27, Chapter 6]. However, the present values were obtained by applying LPC analysis to FFT power spectra of the signals with the algorithm detailed in [20]. The residual waveguide resonances were removed from the spectra before LPC analysis. The results were compared visually to the peaks of the smoothed spectra to detect crude errors. The final results in Table 2 are the averages of these two values, augmented with their half distances. The formant data for [i] is subject to following remarks: (i) the LPC found a peak at 855 ± 133 Hz but this was removed from the data set as an outlier; (ii) F_2 could not be extracted from the beginning sample by the LPC even though it can be found easily in spectral curves by visual inspection; (iii) the LPC finds very strong *double* peaks about 500 Hz apart at F_3, and the F_3-values given in Table 2 are defined as their means.

The data of Table 2 can be found in [26] except [œ] (which is from a different series where $f_0 = 137.5$ Hz) and F_3, F_4 of [i] (which required a higher order LPC run). These results *without* numerical compensation of the residual longitudinal resonances of the waveguides can be found in [27, Tables 6.2 and 6.3 on p.49–50]. We remark that a typical mean deviation in vowel formant frequencies (when measured in ideal conditions in an anechoic chamber rather than inside a MRI machine) is in the class of 0.5 semitones;

Vowel	D_1	D_2	D_3	D_4	mean discr.
[ɑ]	1.7	7.1	0.5	2.0	2.8
[i]	-0.1	-0.4	1.4	1.0	0.7
[u]	1.0	-0.4	0.7	-0.8	0.7
[œ]	2.6	4.4	4.0	2.1	3.3

Table 3: *Discrepancy (in semitones) between computed resonances and mean formant frequencies from Table 2. Positive number implies that the computed resonance is higher than the measured formant.*

see [6].

6 Results and conclusions

Just as in [15], our new data indicates that the computed resonances R_i from (2) tend to be higher than the measured formants F_i. The discrepancy given in Table 3 is in semitone scale to make the comparison easy with the "$3\frac{1}{2}$ semitone rule" that was discovered in [15]. Recall that difference of frequencies F and R is $D = 12\ln(R/F)/\ln(2)$ semitones.

The main sources of discrepancy in these computations and experiments are as follows: (i) less than perfect performance of the test subject in the MRI machine, (ii) sporadic problems in formant extraction by the LPC, and (iii) physically unrealistic boundary conditions in Eqs. (1)–(2) especially at the mouth opening.

The mean discrepancy in Table 3 is at its largest for vowels [ɑ] and [œ] where the computed resonances are consistently higher than the measured formants. Also, the mouth opening is largest for these vowels in our data set, and the Dirichlet boundary condition on Γ_1 in (2) is expected to be the most significant error source. All this is in good agreement with the results and the conclusions of [15].

The particularly significant error in F_2 of [ɑ] can be explained by the fact that the velar port of the subject was unexpectedly open in the MR image, and the anti-node of the standing pressure wave (corresponding to F_2) would be at the velar port *if* it was closed. The nasality of the pronunciation is clearly heard from the speech sample. In the computational geometry, however, the hole was closed manually which leads to the perfectly reflecting Neumann boundary condition for the velar opening. It is physically more realistic to use a similar boundary condition for the velar opening as on Γ_3 in (2).

It is worth noting that the computational model performs strikingly well

for [u]: The discrepance is of the same order as the fluctuations in formant values in sustained vowel production [6]. The velar port is closed in this MRI geometry. Also, the mouth opening is very small which results in relatively smaller error due to the Dirichlet boundary condition.

We conclude that the error profile in Table 3 supports earlier observations in [15], and it can be qualitatively explained by considering the underlying physics. A more sophisticated exterior space model (compared to the Dirichlet boundary condition) is likely to remove most of the formant discrepancy in vowels where the mouth opening is large. Complications related to the open velar port should be treated by taking into account the nasal tract resonating structures. This can be done by including them in the computational geometry or by setting an improved boundary condition at the velar port opening.

The results of [32] support the view that computed and measured resonances of a *plastic model* VT do not differ significantly from each other. Rather than carrying out speech recordings in MRI, the authors produce 3D physical printouts from MRI geometries by fast prototyping techniques for japanese vowels [a], [i], [u], [e], [o]. Separately imaged teeth geometries were manually aligned with the soft tissue geometries. The formant structure is measured from the plastic models in ideal conditions, and the same configuration is used for transfer function simulations by the Finite-Difference Time-Domain (FDTD) method.

It is observed that the formant frequencies of the computed and measured transfer functions differ from each other by less than 3.2% (i.e., 0.55 semitones) which is comparable to our results on vowels [i] and [u]. Such an indirect experimental arrangement excludes most of the sources of discrepancy considered in our work, and the results of [32] can therefore be regarded as a limit what is reasonable to expect in a computational modelling effort of true vowel utterance. The effect of anatomic details such as piriform fossae, epiglottic valleculae and inter-dental spaces were computed, and the contribution of the latter two was found to be almost negligible in [32].

7 Acknowledgements

The authors were supported by the Finnish Academy grant Lastu 135005, the Finnish Academy projects 128204 and 125940, European Union grant Simple4All, Aalto Starting Grant, and Åbo Akademi Institute of Mathematics.

References

[1] A. Aalto. A low-order glottis model with nonturbulent flow and mechanically coupled acoustic load. Master's thesis, Aalto University, Department of Mathematics and Systems Analysis, 2009.

[2] A. Aalto, D. Aalto, J. Malinen, and M. Vainio. Modal locking between vocal fold and vocal tract oscillations. Submitted, 2012.

[3] A. Aalto, P. Alku, and J. Malinen. A LF-pulse from a simple glottal flow model. In *Proceedings of the 6th International Workshop on Models and Analysis of Vocal Emissions for Biomedical Applications (MAVEBA2009)*, pages 199–202, 2009.

[4] A. Aalto and J. Malinen. Composition of passive boundary control systems. *Mathematical Control and Related Fields*, 2012.

[5] D. Aalto, O. Aaltonen, R.-P. Happonen, J. Malinen, P. Palo, R. Parkkola, J. Saunavaara, and M. Vainio. Recording speech sound and articulation in MRI. In *Proceedings of BIODEVICES 2011*, pages 168–173, 2011.

[6] D. Aalto, J. Malinen, M. Vainio, J. Saunavaara, and J. Palo. Estimates for the measurement and articulatory error in MRI data from sustained vowel phonation. In *Proceedings of the International Congress of Phonetic Sciences*, 2011.

[7] T. Chiba and M. Kajiyama. *The Vowel, Its Nature and Structure*. Phonetic Society of Japan, 1958.

[8] K. Dedouch, J. Horáček, T. Vampola, and L. Černý. Finite element modelling of a male vocal tract with consideration of cleft palate. In *Forum Acusticum*, 2002.

[9] K. Dedouch, J. Horáček, T. Vampola, J.G. Švec, P. Kršek, and R. Havlík. Acoustic modal analysis of male vocal tract for Czech vowels. In *Proceedings Interaction and Feedbacks '2002*, pages 13 – 19, 2002.

[10] H. K. Dunn. The calculation of vowel resonances, and an electrical vocal tract. *J. Acoust. Soc. Am.*, 22:740 – 753, 1950.

[11] S. El Masri, X. Pelorson, P. Saguet, and P. Badin. Vocal tract acoustics using the transmission line matrix (TLM) method. In *Proceedings of the 4th International Conference on Spoken Language Processing*, pages 953 – 956, 1996.

[12] S. El Masri, X. Pelorson, P. Saguet, and P. Badin. Development of the transmission line matrix method in acoustics. Applications to higher modes in the vocal tract and other complex ducts. *Int. J. of Numerical Modelling*, 11:133 – 151, 1998.

[13] O. Engwall and P. Badin. Collecting and analysing two- and three-dimensional MRI data for Swedish. *TMH-QPSR*, (3-4/1999):11–38, 1999.

[14] G. Fant. *Acoustic Theory of Speech Production*. Mouton, The Hague, 1960.

[15] A. Hannukainen, T. Lukkari, J. Malinen, and P. Palo. Vowel formants from the wave equation. *J. Acoust. Soc. Am. Express Letters*, 122(1):EL1–EL7, 2007.

[16] H. L. F. Helmholtz. *Die Lehre von den Tonempfindungen als physiologische Grundlage für die Theorie der Musik*. Vieweg, Braunschweig, 1863.

[17] J. Kelly and C. Lochbaum. Speech synthesis. In *Proceedings of the 4th International Congress on Acoustics*, pages Paper G42: 1–4, 1962.

[18] C. Lu, T. Nakai, and H. Suzuki. Finite element simulation of sound transmission in vocal tract. *J. Acoust. Soc. Jpn. (E)*, 92:2577 – 2585, 1993.

[19] T. Lukkari and J. Malinen. Webster's equation with curvature and dissipation. Preprint (downloadable from arXiv), 22 pp. + 5 pp. appendix, 2011.

[20] J. Makhoul. Spectral linear prediction: Properties and applications. *IEEE Transactions on Acoustics, Speech and Signal Processing*, 23(3):283–296, 1975.

[21] J. Malinen and P. Palo. Recording speech during MRI: Part II. In *Proceedings of the 6th International Workshop on Models and Analysis of Vocal Emissions for Biomedical Applications (MAVEBA2009)*, pages 211–214, 2009.

[22] J. Mullen, D. Howard, and D. Murphy. Waveguide physical modeling of vocal tract acoustics: Flexible formant bandwith control from increased model dimensionality. *IEEE Transactions on Audio, Speech and Language Processing*, 14(3):964 – 971, 2006.

[23] M. Niemi, JP Laaksonen, T. Peltomaki, J. Kurimo, O. Aaltonen, and RP Happonen. Acoustic comparison of vowel sounds produced before and after orthognathic surgery for mandibular advancement. *Journal of Oral & Maxillofacial Surgery*, 64(6):910–916, 2006.

[24] T. Niikawa, T. Ando, and M. Matsumura. Frequency dependence of vocal-tract length. In *Proceedings of the 7th International Conference on Spoken Language Processing*, pages 1525 – 1528, 2002.

[25] H. Nishimoto, M. Akagi, T. Kitamura, and N. Suzuki. Estimation of transfer function of vocal tract extracted from MRI data by FEM. In *The 18th International Congress on Acoustics*, volume II, pages 1473 –1476, 2004.

[26] J. Palo, D. Aalto, O. Aaltonen, R.-P. Happonen, J. Malinen, J. Saunavaara, and M. Vainio. Articulating Finnish vowels: Results from MRI and sound data. *Linguistica Uralica*, 2012.

[27] P. Palo. *A wave equation model for vowels: Measurements for validation.* Licentiate thesis, Aalto University, Department of Mathematics and Systems Analysis, 2011.

[28] N. Rofsky, V. Lee, G. Laub, M. Pollack, G. Krinsky, D. Thomasson, M. Ambrosino, and J. Weinreb. Abdominal mr imaging with a volumetric interpolated breath-hold examination. *Radiology*, pages 876–88, 1999.

[29] K. Sasaki, N. Miki, and Y. Miyanaga. FEM analysis based on 3-D time-varying vocal tract shape. In *EUROSPEECH-2003*, pages 2357 – 2360, 2003.

[30] H. Si. http://tetgen.org/, 2011. Accessed Feb. 13th, 2012.

[31] M. M. Sondhi. Resonances of a bent vocal tract. *J. Acoust. Soc. Am.*, 79(4):1113–1116, 1986.

[32] H. Takemoto, P. Mokhtari, and T. Kitamura. Acoustic analysis of the vocal tract during vowel productions by finite-difference time-domain method. *J. Acoust. Soc. Am.*, 128(6):3724–3738, 2010.

[33] K. Vahatalo, JP Laaksonen, H. Tamminen, O. Aaltonen, and RP Happonen. Effects of genioglossal muscle advancement on speech: an acoustic study of vowel sounds. *Otolaryngology - Head & Neck Surgery*, 132(4):636–640, 2005.

[34] P. Švancara and J. Horáček. Numerical modelling of effect of tonsillectomy on production of Czech vowels. *Acta Acustica united with Acustica*, 92:681 – 688, 2006.

[35] P. Švancara, J. Horáček, and L. Pešek. Numerical modelling of production of Czech wovel /a/ based on FE model of the vocal tract. In *Proceedings of International Conference on Voice Physiology and Biomechanics*, 2004.